The Astrophysical Journal, 705:1–8, 2009 ??? doi:10.1088/0004-637X/705/1/1

RADIATION FROM COMOVING POYNTING FLUX ACCELERATION

Edison Liang and Koichi Noguchi
Rice University, Houston TX 77005-1892, USA
Received 2007 May 7; accepted 2009 September 30; published 2009 ???

ABSTRACT

We derive analytic formulas for the radiation power output when electrons are accelerated by a relativistic comoving kinetic Poynting flux, and validate these analytic results with particle-in-cell simulations. We also derive analytically the critical frequency of the radiation spectrum. Potential astrophysical applications of these results are discussed. A quantitative model of gamma-ray bursts based on the breakout of kinetic Poynting flux is presented.

Key words: acceleration of particles – gamma rays: bursts – radiation mechanisms: non-thermal

Online-only material: color figures

1. INTRODUCTION

In popular paradigms of radiation from blazars, pulsar wind nebulae (PWN), and gamma-ray bursters (GRB), relativistic outflow energy (hydrodynamic or electromagnetic) from the central compact object (black hole or neutron star) is first converted into relativistic nonthermal kinetic energy of electrons via some dissipation mechanisms (e.g., collisionless shocks, Dermer 2003; Meszaros 2002; Lyubarsky 2005). These nonthermal electrons are then hypothesized to radiate, in the comoving frame of the outflow, synchrotron-like radiation (Rybicki & Lightman 1979; Epstein & Petrosian 1973; Lloyd & Petrosian 2000), or "jitter" radiation if the magnetic field is too chaotic (Weibel 1958; Medvedev 2000; Medvedev et al. 2005). In addition, inverse comptonization of the internal synchrotron (SSC) or external soft photons (EC), plus hadronic processes, may produce the high-energy gamma rays (Dermer et al. 2000, 2003). However, the kinetic processes, which convert the outflow energy into nonthermal electron energy and radiation (Hoshino et al. 1992; Gallant et al. 1992; Silva et al. 2003; Nishikawa et al. 2003; Spitkovsky 2008; Smolsky & Usov 2000; Lyutikov & Blackman 2002; Van Putten & Levinson 2003; Lyutikov & Blandford 2003), remain unsolved. In this paper, we present a quantitative example of particle acceleration by a comoving Poynting flux (CPF), in which both the radiation power output and critical frequency can be derived analytically. We show that in this case the intrinsic radiation efficiency is very low compared to classical synchrotron theory in a static field. As a result, electrons can be accelerated to very high Lorentz factors before radiation damping sets in.

In addition to the analytic theory, we have performed multidimensional particle-in-cell (PIC) simulations (Langdon & Lasinski 1976; Birdsall & Langdon 1991; Langdon 1992) to model the nonthermal electron acceleration and radiation processes (Liang et al. 2003; Liang & Nishimura 2004; Nishimura et al. 2003; Liang & Noguchi 2005, 2006). In PIC simulations, time is expressed in units of electron plasma frequency and space is expressed in units of plasma skin depth. All physical variables (e.g., electric and magnetic fields) are nondimensionalized by the electron density which is left arbitrary since the plasma is assumed to be Birdsall & Langdon 1991 collisionless (see Birdsall & Langdon 1991). A unique feature of our PIC simulations is that the intrinsic power radiated by each superparticle (= numerical representation of a charged particle) can be computed simultaneously as the superparticle is accelerated by the local Lorentz force (Noguchi et al. 2005; Liang & Noguchi 2005, 2006). Such simulation provides a fully self-consistent treatment of the intrinsic radiation power during the acceleration process. We will calibrate and validate our analytic results using the PIC simulations. Section 2 reviews the basic physics of comoving PF acceleration (CPFA, this term replaces the acronyms DRPA and TPA used in our early papers). In Section 3, we derive the analytic formula for the radiation power output. Section 4 compares the analytic results with the numerical radiation power from PIC simulations. In Section 5, we derive analytically the critical frequency of CPFA radiation. In Section 6, we discuss the astrophysical applications of the above results. In Section 7, we apply the analytic formulas to a simplified PF model of long GRBs. Section 8 is devoted to discussions and summary.

2. COMOVING POYNTING FLUX ACCELERATION (CPFA)

In this paper, we define "Poynting flux" (PF) narrowly as a kinetic plasma outflow dominated and accelerated by *transverse* electromagnetic (EM) fields with $\Omega_e/\omega_{pe} = B/(4\pi nm)^{1/2} > 1$, without the presence of flow-aligned guiding magnetic fields ($\Omega_e = eB/m$ = electron gyrofrequency, $\omega_{pe} = (4\pi ne^2/m)^{1/2}$ = electron plasma frequency, m = electron mass, n = electron density; we set $c = 1$ throughout this paper except in Sections 6 and 7). Hence particle acceleration by classical Alfven and whistler waves (Boyd & Sanderson 1969, see discussions in Section 8) in a background magnetic field, or by longitudinal plasma (Langmuir) waves (Tajima & Dawson 1979) will not be considered in this paper. Instead we focus on semi-coherent particle acceleration by the ponderomotive ($J\times B$) force of a comoving PF (Liang et al. 2003). Astrophysical examples of such relativistic PF include the equatorial stripe wind of pulsars and magnetars (Lyubarsky 2005, Skjaeraasen et al. 2005), and the low-density limit of a magnetic tower jet driven by strongly magnetized accretion disks around black holes (Koide et al. 2004). More examples will be discussed in Sections 6 and 7.

Comoving PF acceleration (CPFA) occurs when an intense EM pulse, loaded with a small amount of plasma, maintains a *group* velocity ($<c$ due to plasma loading) roughly in phase with the fastest electrons. As slower electrons gradually fall behind the EM pulse, the plasma loading of the main EM pulse decreases, the "group velocity" of the pulse accelerates, and the Lorentz factor of the remaining comoving electrons increases,

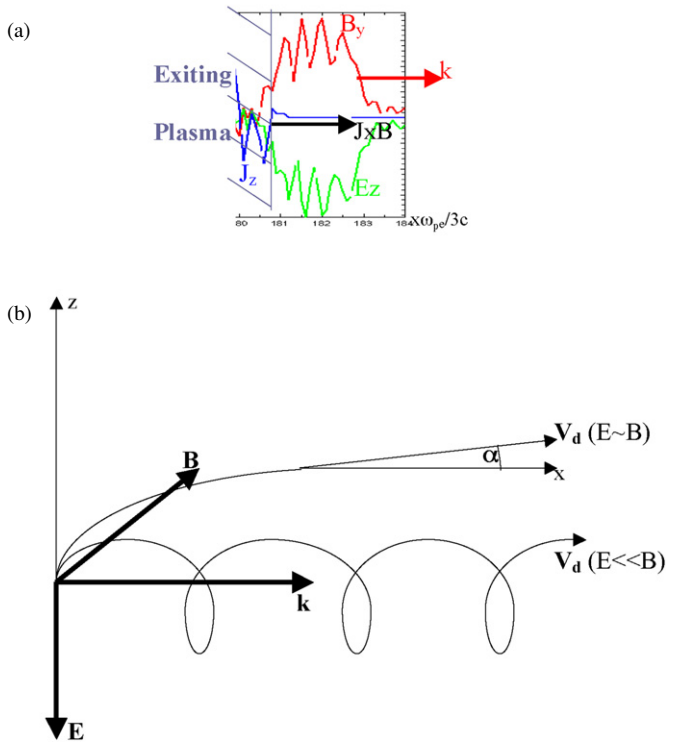

Figure 1. (a) Picture illustrating the CPFA concept. In all figures of this paper, t is divided by $3/\omega_{pe}$, and x is divided by $3c/\omega_{pe}$. An intense plane EM pulse escaping from an overdense plasma induces a polarization current, so that the $J\times B$ force pulls out the surface electrons relativistically. But only the fastest electrons can keep up with the EM pulse. So the plasma loading of the EM pulse decreases with time. This leads to sustained acceleration of only the fast electrons, with no limit to their Lorentz factor. The sharp plasma boundary (hatched) is sketched only for illustration. Actual simulations using smooth density profiles achieve similar asymptotic results. (b) CPFA can also be visualized in terms of $E \times B$ drift in a comoving EM pulse. As $|E| ==> |B|$, the particle path becomes quasi-rectilinear. α is the asymptotic angle between the Poynting vector **k** and the drift velocity v_d.

(A color version of this figure is available in the online journal.)

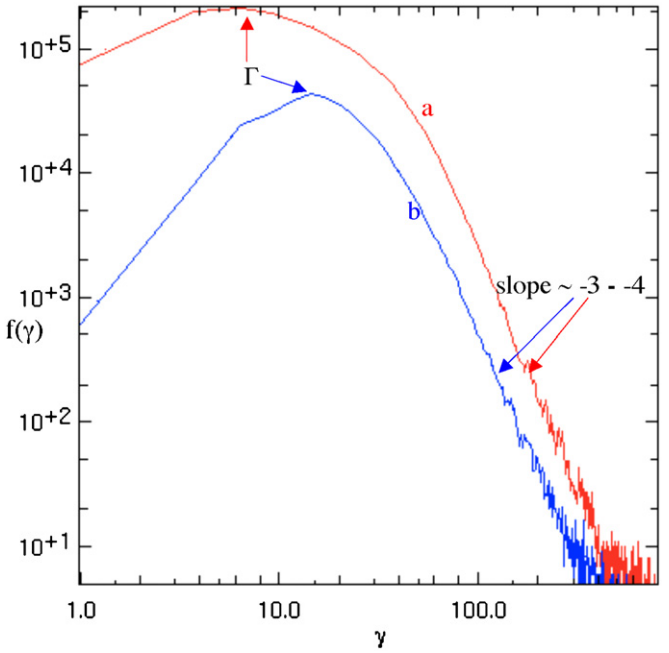

Figure 2. (a) Asymptotic electron energy distribution function $f(\gamma)$ in the main pulse of two sample CPFA runs. Two plane slabs of magnetic-dominated pair plasma with initial $kT_o = 0.125$ m and $\Omega_e/\omega_{pe} = 10$ were allowed to freely expand into a vacuum with different initial thicknesses: (cf. Liang et al. 2003) (a) $L_o = 10^4\ c/\omega_{pe}$ and (b) $L_o = 10^3\ c/\omega_{pe}$. Both pulses develop robust power-law electron spectra of slope from ~ -3 to -4 with low-energy turnovers at Γ. Spectrum (a) was obtained after $t = 10\ L_o/c$. Spectrum (b) was obtained after $t = 100\ L_o/c$, when the pulse "group velocity" Lorentz factor reached $\gamma_w \sim \Gamma \sim 15$. It took several million time steps of PIC simulations to achieve such well-defined power-law electron distributions.

(A color version of this figure is available in the online journal.)

until dephasing or radiation damping sets in eventually. The net effect is that the PF transfers its energy and momentum to a *decreasing* number of faster electrons over time (Liang & Nishimura 2004, LN04 hereafter). A physical realization of CPFA was discovered by Liang et al. (2003) using PIC simulations. When a slab of strongly magnetized $(B/(4\pi nm)^{1/2} > 1)$ overdense ($\omega_{pe} > 2\pi/\lambda$, λ = characteristic wavelength of the EM pulse) plasma expands into a vacuum or low-density region, the initial expansion disrupts the sustaining current, leading to $4\pi J <$ Curl B. The excess displacement current $(\partial \mathbf{E}/\partial t)$ then generates a transverse EM pulse, which tries to escape from the embedding plasma. As the EM pulse tries to escape, it "pulls" out the surface electrons via the $J\times B$ force (Figure 1(a)), where J is the self-induced polarization current (Boyd & Sanderson 1969). When the $J\times B$ force is very strong, the accelerated electrons can stay *comoving* with the *group* velocity of the EM pulse, and the acceleration becomes semi-coherent and self-sustaining (Liang et al. 2003; Liang & Nishimura 2004, LN04 hereafter; Liang 2005). CPFA can also be understood in terms of relativistic $E\times B$ drift in an intense EM pulse. As the drift velocity v_d approaches c, the electron moves almost along a straight line instead of cycloids (Figure 1(b)). Provided that the plasma loading decreases with time due to the loss of slow particles, the EM pulse will accelerate, approaching a vacuum EM wave as $|E/B|$ increases towards unity. This leads to continuous acceleration of v_d.

Using PIC simulations, LN04 found that the maximum Lorentz factor achievable by CPFA grows without limit as $\sim(\Omega_e t)^{1/2}$ until radiation damping or dephasing (e.g., due to wave-front curvature) sets in. LN04 also found that the CPF asymptotically accelerates the high-energy electrons into a simple power law of slope from -3 to -4, independent of the initial conditions or the pulse size (Figure 2). CPFA is exceedingly robust and efficient, capable of converting >50% of the EM energy into accelerated particle energy over a distance $\sim$ a few times the initial pulse width (see Section 7). In contrast to shocks (Spitkovsky 2008; Silva et al. 2003), in which the bulk flow energy is converted into turbulent EM energy and internal particle heat, CPFA converts ordered EM energy directly into accelerated particle energy via continuous rarefaction of the plasma density. The detailed physics of CPFA has been reviewed extensively elsewhere (Liang 2005; Liang & Noguchi 2005), so they will not be repeated here.

3. RADIATION POWER EMITTED BY CPFA

In this section, we derive an analytic approximation for the power radiated by an electron accelerated kinetically by a CPF. The following derivation assumes linearly polarized plane EM waves for simplicity, but the results should be valid in general three-dimensional geometry as long as the wave-front curvature and transverse gradients are $\ll 1/$(acceleration distance). We emphasize that the radiation formula derived in this section should be applicable to any particle accelerated by transverse EM fields comoving with the local **ExB** drift velocity v_d. Hence its potential astrophysical applications should be much broader than the simplified CPFA scenarios discussed above.

Since the radiation power output (energy/sec) is a Lorentz invariant, one way to derive the power radiated is to start with the classical synchrotron formula (Rybicki & Lightman 1979) in a (primed) local Lorentz frame in which $\mathbf{E}' = 0$ and $\mathbf{B}'$ is static, and then use appropriate Lorentz transformations to express the power in terms of lab-frame quantities. However, we find it to be more transparent to work directly in the lab-frame. It turns out to be also more convenient to discuss the different limiting cases and approximations if we derive the radiation power using lab-frame quantities. This is the approach we adopt in the following.

The relativistic dipole radiation power is given by (Rybicki & Lightman 1979):

$$P_{\rm rad} = 2e^2(F_{||}^2 + \gamma^2 F_{+}^2)/3m^2 \quad (1)$$

where γ = Lorentz factor, $F_{\|}$ = force component along velocity $\mathbf{v}$, and F_+ = force component orthogonal to $\mathbf{v}$. For particle motion in a linearly polarized plane EM wave with $(E, B) = (E_z, B_y)$ (Figure 1(b), note that E_z is negative), we have the Lorentz force: $F_x = -ev_z B_y$; $F_y = 0$; $F_z = e(E_z + v_x B_y)$. Here x is the direction of the Poynting vector $\mathbf{k}$. After a little algebra, we find

$$F_{||} = eE_z v_z/v; \quad F_+^2 = e^2 B_y^2[\sin^2\alpha(v^2 - v_w^2) + (v_x - v_w)^2], \quad (2)$$

where $v_w = -E_z/B_y$ is the local "profile speed" of the EM field ($v_w < 1$ due to plasma loading) and $\sin\alpha = v_z/v = p_z/p$. Substituting Equation (2) into Equation (1), we obtain

$$P_{\rm analytic} = 2e^4 B_y^2[\sin^2\alpha(\gamma^2 - 1)(1 - v_w^2) + \gamma^2(v_x - v_w)^2]/3m^2. \quad (3)$$

In addition to B_y and γ, the instantaneous power radiated by an EM-wave-accelerated electron thus depends on two key parameters: the local EM field profile speed v_w and the angle α (we emphasize that α is not the pitch angle, Rybicki & Lightman 1979). Equation (3) reduces to the classical synchrotron formula $P_{\rm syn} = 2e^4 B_y^2 \gamma p_+/3m^2$ (p_+ is the component of p orthogonal to B, Rybicki & Lightman 1979) in the static limit $v_w = 0$ and simplifies in various other limits as follows.

1. *Comoving particles* ($v_x = v_w$). In this case, Equation (3) simplifies to $P_{\rm analytic} = 2e^4 B_y^2(p_z^2 + p_y^2)\sin^2\alpha/3m^2$ when $\gamma \gg 1$. Since in all CPFA runs, $p_z \gg p_y$ (p_y is conserved) at late times (see below), this reduces to

$$P_{\rm analytic} = 2e^4 B_y^2 p_z^2 \sin^2\alpha/3m^2 = 2e^4 B_y^2 p^2 \sin^4\alpha/3m^2 \times \sim 2e^4 B_y^2 \gamma^2 \sin^4\alpha/3m^2. \quad (4)$$

   However, Equation (4) is not a good approximation for electrons significantly out of phase with v_w (note that electrons can have $v_x > v_w$ or $v_x < v_w$). Using PIC simulations, Liang & Nishimura (2004) showed that the peak of the EM pulse moves with profile velocity v_w close to the peak γ of the particle distribution function $f(\gamma)$ of the main EM pulse (cf. Figure 2).
2. *Vacuum pulse limit* ($v_w = 1$). In the limit $v_w = 1$, the PF propagates as a vacuum EM wave. Equation (1) becomes, for $\gamma \gg 1$:

$$P_{\rm analytic} = 2e^4 B_y^2 \gamma^2(1 - v_x)^2/3m^2 \sim e^4 B_y^2 \gamma^2 \sin^4\alpha/6m^2. \quad (5)$$

   Equation (5) has the same functional form as Equation (4), but its magnitude is a factor of 4 lower. It defines the *lower limit* to the radiative power loss of a PF-accelerated electron, since in practice $v_w < 1$.
3. *Slightly subluminal PF* ($1 - v_w = \varepsilon \ll 1$). For most astrophysics applications, the PF will be slightly subluminal. We can simplify Equation (3) by Taylor expanding $1 - v_w = \varepsilon \ll 1$ to the lowest order. This gives rise to

$$P_{\rm analytic} \sim 2e^4 B_y^2 \gamma^2(\varepsilon + \sin^2\alpha/2)^2/3m^2. \quad (6)$$

   For a relativistic CPFA, both ε and $\sin\alpha$ are $\ll 1$. Hence $P_{\rm analytic} \ll P_{\rm syn}$. This is because CPFA acts like a quasi-linear accelerator. Equation (6) shows that $P_{\rm analytic}$ behaves differently depending on whether $\varepsilon \gg$ or $\ll \sin^2\alpha/2$. In the former case, $P_{\rm analytic}$ depends solely on the EM field profile speed v_w and not on α:

$$P_{\rm analytic} \sim 2e^4 B_y^2 \gamma^2 \varepsilon^2/3m^2. \quad (7)$$

   In the latter case, we regain the vacuum limit Equation (5) which depends only on α and not on v_w. We note that the comoving limit Equation (4) is retrieved when $\varepsilon = \sin^2\alpha/2$. When we model astrophysical data using these formulas, we obtain different (B, γ) values depending on the values of ε and $\sin\alpha$, which depends on the PF initial conditions. Equations (4), (5), and (7), which contain only three unknowns, (B, γ, α) or (B, γ, ε) are easier to use for modeling astrophysical data than Equation (3) or (6), which contains four unknowns. The three unknowns are analogous to the conventional synchrotron model with three unknowns B, γ and the pitch angle θ between B and p. However, unlike the pitch angle θ, which can be arbitrary, we find that $\sin\alpha$ lies in a narrow range for the most radiative CPFA particles (Figure 6). We emphasize that the cause of low radiation power of small pitch angle synchrotron radiation (Epstein & Petrosian 1973) is fundamentally different from CPFA radiation: $p//B$ as θ ==> 0, whereas p is orthogonal to B as α ==> 0. CPFA has low radiative power because the particle track is rectilinear due to relativistic, comoving B, not due to $p//B$. Equation (6) is most useful in the ultra-relativistic regime $\varepsilon \ll \sin^2\alpha/2$, which seems to be the case for GRBs (cf. Section 7) and may also be the case for blazars and PWNs. In the following section, we will compare the above analytic approximations with PIC simulation results, which span a dynamic range of 10^5.

4. NUMERICAL RADIATION POWER OUTPUT

In this section, we present the intrinsic radiation output of electrons (and positrons) accelerated by a kinetic CPF using 2.5D (two-dimensional space, 3 momenta) PIC simulations and compare them to the analytic formulas of the last section. We compute the radiation power output by incorporating the relativistic dipole formula Equation (1) into our PIC code. Numerically, we compute the power radiated by each superparticle by interpolating the EM field data from the cell boundaries to the instantaneous superparticle position, so that F and v refer to the *same time and space* point (Noguchi et al. 2005). This is a nontrivial procedure since in PIC simulations, particle and field data are offset by half time steps, and different field variables are offset by half grid spaces (Birdsall & Langdon 1991; Langdon & Lasinski 1976). We have carefully calibrated this numerical procedure with known analytic results. Figure 3 compares the PIC-simulated radiation output for an isotropic thermal plasma (kT = 10 m) in a static uniform B field, with that computed from the analytic synchrotron formula (Rybicki & Lightman 1979). Their good agreement for the high-power electrons validates our basic numerical algorithm. The scatter at low powers

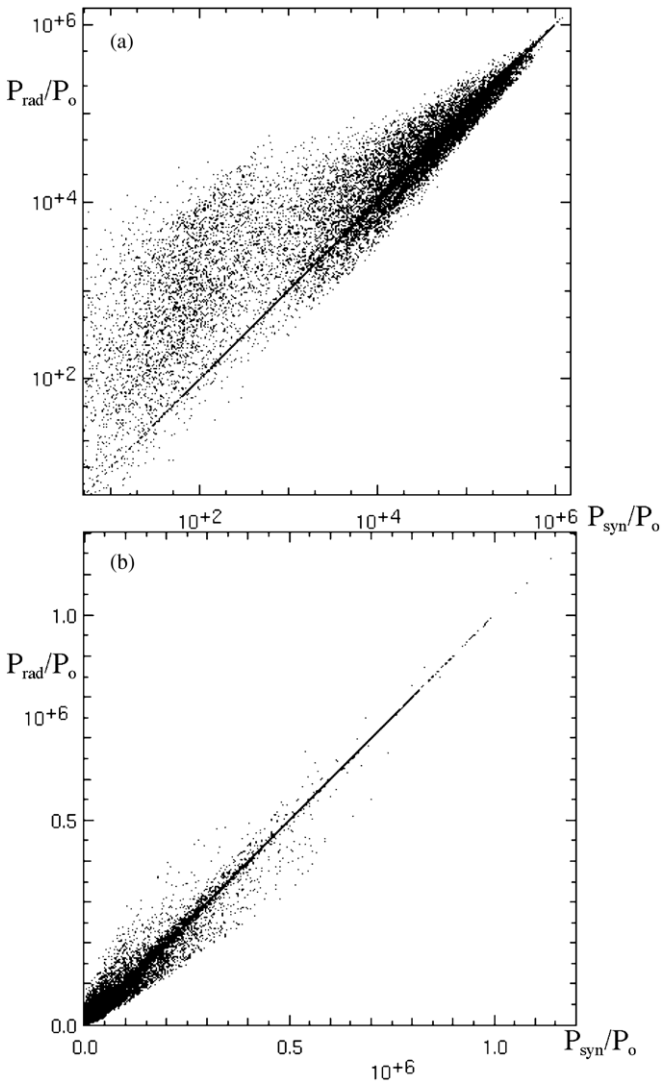

Figure 3. Calibration of the numerical radiation power $P_{\rm rad}$ computed from PIC simulation (Equation (1)) against the analytic synchrotron formula $P_{\rm syn}$ for a kT = 5 MeV thermal plasma in a static uniform B field shows good agreement at high powers in both (a) log–log and (b) linear–linear plots. The discrepancy and scatter at lower powers are mainly due to numerical errors from interpolating the field values from cell boundaries to the particle position. However, for an ensemble of particles, the total power output is dominated by the high power particles. Throughout this paper, all radiative powers ($P_{\rm rad}$, $P_{\rm syn}$, and $P_{\rm analytic}$) are normalized by $P_o = 2e^2\Omega_{\rm e}{}^2/2700$.

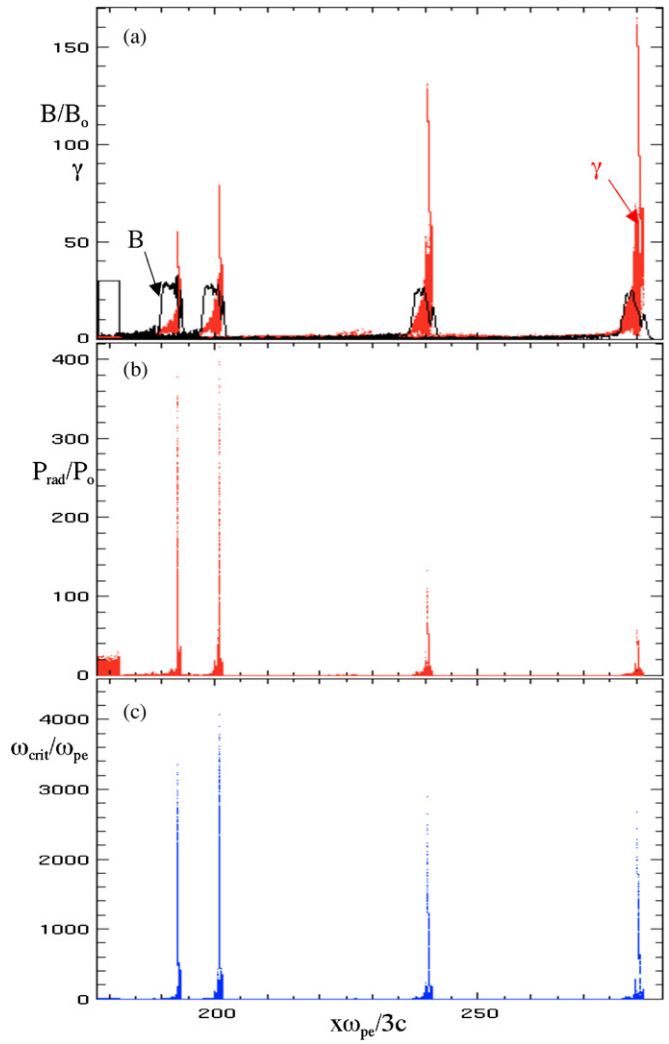

Figure 4. Snapshots at different times of the spatial profiles of a pair-loaded EM pulse propagating from left to right show the CPFA evolution. The e^+e^- plasma slab has initial temperature $kT_{\rm o}$ = 0.005 m, pulse width $L_o = 12\ c/\omega_{pe}$, $\Omega_{\rm e}/\omega_{pe} = 10$, and was initially located at $x\omega_{pe}/3c = 180$. The five snapshots (left to right) are taken at $t\omega_{pe}/3 = 0$, 12, 20, 60, 100. We show the scatter plot for 1% of all superparticles. (a) Time evolution of the magnetic field B_y and electron Lorentz factors γ spatial distributions shows monotonic increase in γ and conversion of magnetic energy into particle energy via current dissipation. (b) Evolution of $P_{\rm rad}$ spatial distribution shows that radiation loss for the highest energy electrons peaks at ~5 light crossing times, followed by monotonic decay when the increase in γ is countered by the decrease in B and sinα. (c) Evolution of the critical frequency $\omega_{\rm cr}$ spatial distribution shows a similar trend. $\omega_{\rm cr}$ is expressed in units of $\omega_{pe} = 0.1\Omega_e$.

(A color version of this figure is available in the online journal.)

is due to the small but finite errors in the field interpolation procedure. However, PIC simulation data cannot be used directly to compute the radiation spectrum numerically because the PIC time step (typically = 0.25 gyroperiod) is too large to accommodate high frequencies in Fourier transforms. Instead, one has to smoothly interpolate the particle tracks to perform the Fourier transform—an exercise beyond the scope of this paper (see Hededal 2005).

Figure 4 highlights the time evolution of the spatial profiles of field and particle momenta of a typical CPFA run. A linearly polarized plane EM pulse accelerates a slab of overdense e^+e^- plasma from left to right, similar to the case studied by Liang & Nishimura (2004). While the energies of the pairs increase monotonically due to the CPFA (Figure 4(a)), the power radiated by the electrons rises to a maximum after ~5 light transit times of the initial pulse width, but then declines monotonically (Figure 4(b)) due to the trade-off between increasing γ and decreasing B and α. At late times (not shown) $P_{\rm rad}$ approaches a constant value. In Figure 5, we compare the numerical $P_{\rm rad}$ with $P_{\rm analytic}$ of Equation (4) for a different CPFA run (45° line). It shows good correlation for the highest power particles, suggesting that these particles are comoving. At lower power, the scatter plot forms two separate bands lying above and below the 45° line, corresponding to non-comoving electrons with $\varepsilon > \sin^2\alpha/2$ and $\varepsilon < \sin^2\alpha/2$ in Equation (6), respectively. Figure 6 shows the distribution of $P_{\rm rad}$ versus sinα for three sample CPFA runs of different initial temperatures. It shows that the highest power particles have their sinα values concentrated between 0.01 and 0.2. This narrow range of sinα distribution seems to hold up in all our CPFA runs so far. In contrast, in small pitch angle synchrotron radiation (Epstein & Petrosian 1973), θ is arbitrary and uncorrelated with γ.

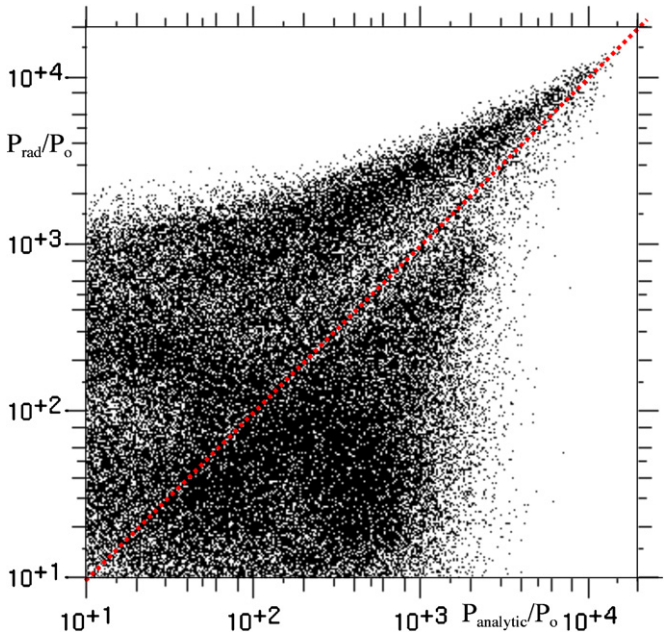

Figure 5. Scatter plot of $P_{\rm rad}$ vs. $P_{\rm analytic}$ of Equation (4) (comoving limit) for a pair plasma CPFA run with initial $\Omega_e/\omega_{pe} = 10$ and $kT_o = 10$ m. We see that the two powers converge only for the highest power particles. As expected at lower power $P_{\rm rad}$ deviates from Equation (4) by a large amount. The scatter is concentrated in two bands above and below the 45° line. These deviations from Equation (4) are due to electrons moving slower or faster than the EM pulse, with $\varepsilon > \sin^2\alpha/2$ and $\varepsilon < \sin^2\alpha/2$, respectively, in Equation (6).

(A color version of this figure is available in the online journal.)

In the PIC simulations presented above, we have ignored radiation reaction due to its very small magnitude (radiation reaction force $\ll$ Lorentz force as long as $B \ll 10^{15}$ G = the Dirac limit). However, our PIC simulations are also capable of including the radiation reaction force term if necessary (Noguchi et al. 2005).

5. CRITICAL FREQUENCY OF CPFA RADIATION

A prominent feature of GRB and blazar radiation spectra is the presence of a low-energy spectral break E_{pk} (hundreds of keV for classical GRBs, radio-IR for blazars). This spectral break is an indicator of the overall spectral hardness and is usually interpreted as the critical frequency of synchrotron radiation $\omega_{\rm crsyn} \sim 1.5\Omega_e\Gamma p_+$ (Rybicki & Lightman 1979) emitted by electrons at the low-energy cutoff Γ (Figure 2). This interpretation of the spectral break, plus the assumption of energy equipartition, is often used to constrain the Lorentz factor and magnetic field of the source. However, as we show below, for radiation emitted by CPFA electrons, the asymptotic critical frequency $\omega_{\rm cr}$ is $\ll\omega_{\rm crsyn}$ due to the quasi-rectilinear motion.

To derive the formula for $\omega_{\rm cr}$, we follow the approach of Landau & Lifshitz (1980): $\omega_{\rm cr}$ is determined by the time measured in the detector frame it takes the radiation beam of opening angle $1/\gamma$ to sweep past the detector due to the curvature of the particle trajectory. For electrons comoving or almost comoving with the PF, the parallel momentum p_x (x is the direction along **k**, Figure 1(a)) increases monotonically, while p_z (momentum along E) asymptotes to a constant (Liang & Nishimura 2004, note that p_y along B is conserved to first order). Hence the change in the radiation beam direction due to the slow bending of particle trajectory is dominated by the change in p_x: $\Delta\theta \sim p_z\Delta p_x/{p_x}^2$. From the Lorentz force equation, we have $d\gamma/dt = eE_z p_z/m\gamma$. Hence the time in the laboratory

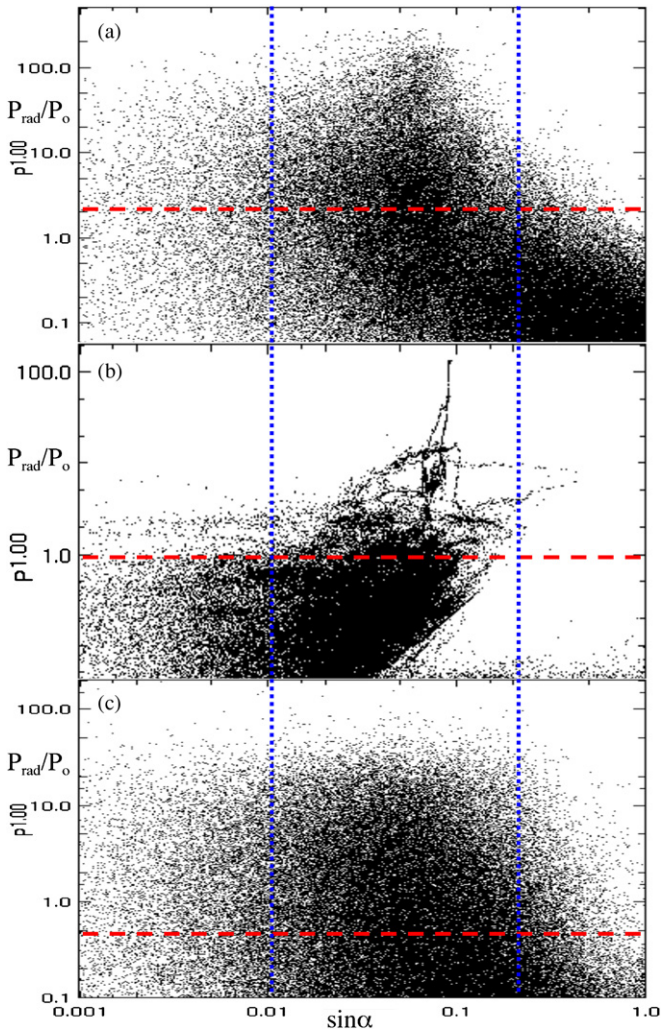

Figure 6. Scatter plots of the distribution of $P_{\rm rad}$ vs. $\sin\alpha$ at late times for three sample pair plasma CPFA runs with initial $\Omega_e/\omega_{pe} = 10$ and $kT_o =$ (a) 10 m; (b) 0.005 m; (c) 0.125 m. Horizontal dash lines denote $P_{\rm rad} = 1\%$ of the maximum emitted power. Most high power electrons lie in the range $0.01 \leqslant \sin\alpha \leqslant 0.2$ (vertical dotted lines).

(A color version of this figure is available in the online journal.)

frame for the radiation beam to change by an angle $\Delta\theta \sim 2/\gamma$ is $\Delta t = 2\gamma^2 m/(eE_z p_z^2)$, where we have used the approximation $\gamma \sim p_x(\gg p_z, p_y)$. This translates into a duration in the detector frame $\Delta t_{ob} = \Delta t/2\gamma^2 = m/eE_z p_z^2$. Thus, the critical frequency (Rybicki & Lightman 1979)

$$\omega_{\rm cr} = 1.5/\Delta t_{\rm ob} = 1.5eE_z p_z^2/m = 1.5\Omega_e p_z^2 \sim 1.5\Omega_e\gamma^2\sin^2\alpha \times \sim \omega_{\rm crsyn}\sin^2\alpha. \quad (8)$$

Since $\sin\alpha \ll 1$ at high power (Figure 6), $\omega_{\rm cr} \ll \omega_{\rm crsyn}$. In Section 7, we will discuss the implications of this result for modeling GRB spectral data. In Figure 4(c), we show the time evolution of $\omega_{\rm cr}$ for the same CPFA run as in Figures 4(a) and (b). It shows that $\omega_{\rm cr}$ follows the same trend as $P_{\rm rad}$, reaching a maximum after a few light transit times of the pulse width. However the decline of $P_{\rm rad}$ is more rapid than $\omega_{\rm cr}$ due to the extra factors of $\sin\alpha$.

6. ASTROPHYSICAL APPLICATIONS

One of the most important applications of the above results to astrophysics is the extraction of the (B, γ) values of the emission

region from observational data. Conventional synchrotron models determine (B, γ) via additional ad hoc assumptions such as energy equipartition, and injection rates of nonthermal electrons (Dermer & Boettcher 2002). In contrast, the CPFA model tightly constrains (B, γ) from first principles because the electron acceleration rate is determined by the PF magnetic field. Liang & Nishimura (2004) derived, using the comoving Lorentz equation, the acceleration rate for CPFA electrons in the lab frame:

$$d\gamma/dt = f\Omega_e/\gamma, \tag{9}$$

where f is a fudge parameter of O(1) that depends only weakly on the initial PF magnetization Ω_e/ω_{pe}. This local acceleration rate is independent of the global properties of the plasma or details of the EM pulse profile. By equating Equation (9) to the radiation loss rate of Section 3, we can now express the asymptotic limiting Lorentz factor $\gamma_{\max}$ of CPFA electrons due to radiation damping:

$$\gamma_{\max} = (3fm^2/(2Be^3 \sin^4 a))^{1/3}. \tag{10}$$

For a given B field, Equation (10) predicts a Lorentz factor much higher than limits from classical synchrotron radiation damping since $\sin\alpha \ll 1$. Equation (10), together with Equation (8) for the critical frequency, allows us to determine (B, γ) uniquely from the spectral break energy E_{pk} (modulo the small uncertainty in f and $\sin\alpha$), without invoking energy equipartition, particle injection rate or other ad hoc assumptions. In this sense, the CPFA model is more constraining and predictive than conventional synchrotron models, which do not specify the particle acceleration mechanism or the acceleration rate. In Section 7, we will apply Equations (10) and (8) to a PF model of GRBs. As a PF pulse evolves, B decreases (Figure 4) due to conversion of EM energy into particle energy (cf. Figure 7). Hence $\gamma_{\max}$ increases with time. However, CPFA ceases to operate after B drops too low so that $\Omega_e < \omega_{pe}$.

CPFA may be relevant to astrophysics in two different settings: global and local. Globally, macroscopic EM pulses with ordered fields and low plasma loading may be generated by magnetic tower jets or transient magnetar winds (Koide et al. 2004) emerging from collapsars, or from the merger of strongly magnetized neutron stars into a black hole or ms magnetar. For example, CPFA can take place when a magnetic tower jet punches through a collapsar envelope or wind, and converts MHD waves into a kinetic EM pulse at sufficiently low ambient density (see Section 7). Similarly, when a millisecond magnetar collapses into a black hole, or when a strongly magnetized neutron star binary merges to form a black hole, part of its collapse energy may be emitted in the form of an intense EM pulse.

Alternatively, CPFA may also occur at the local level in the absence of large-scale-ordered EM fields. For example, magnetic-dominated (high-σ) turbulence generated by relativistic shear layers, shocks or reconnection, may dissipate locally via the CPFA mechanism when nonlinear EM waves propagate into low-density regions with $\Omega_e > \omega_{pe}$. In this case, CPF acceleration persists only until dephasing occurs due to wave-front curvature and inhomogeneity. So the maximum Lorentz factor achieved may be much lower than the radiation damping limit given by Equation (10).

7. APPLICATION TO A PF MODEL OF LONG GRBS

Currently there is no universally accepted model of GRB energization and radiation. Two popular paradigms are hydrodynamic or electromagnetic outflows from a central engine (e.g., a newly formed black hole accretion disk or millisecond magnetar), dissipating at a distance of 10^{14-15} cm (Meszaros 2002; Piran 2000). Recent Fermi observation of the ultra-luminous GRB080916c which fits a simple "band function" spectrum extending from soft X-rays to >100 GeV (Abdo et al. 2009) may favor a PF origin (Zhang 2009). If GRB is indeed energized by an intense PF outflow, CPFA would be an attractive dissipation mechanism due to its high-energy conversion efficiency (Figure 7) and universal power-law spectra with low-energy turnover (Figure 2). Here we apply the analytic formulas of the previous sections to a simple quantitative model of long GRBs, assuming that the PF contains only e^+e^- pairs with no ions (e–ion models will be considered in future papers). Using the CPFA model, we can predict the spectral break energy $E_{\rm pk}$ from first principles, which has not been achieved in conventional synchrotron shock models.

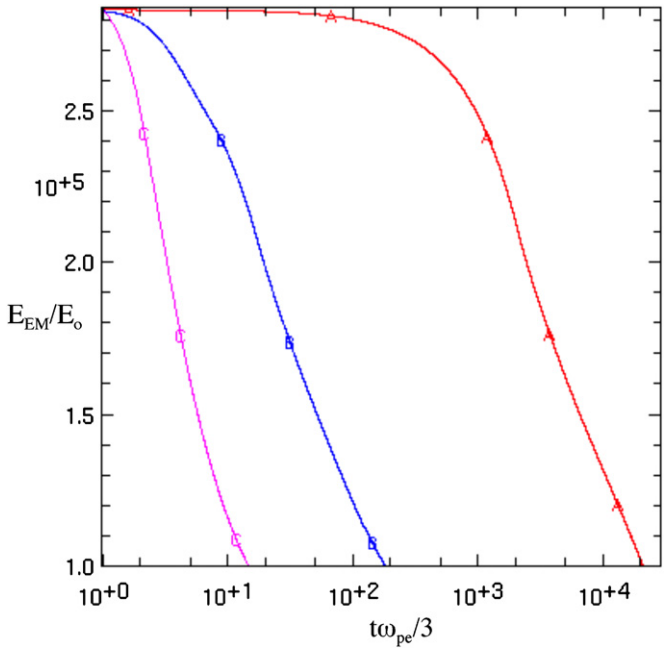

Figure 7. Decay of EM energy for $\Omega_e/\omega_{pe} = 10$, $kT_o = 10$ m CPFA pair plasma runs with three different initial pulse widths: (1) $L_o = 10800\ c/\omega_{pe}$; (2) $L_o = 90\ c/\omega_{pe}$; (3) $L_o = 12\ c/\omega_{pe}$. These results show that the time to convert 50% of EM energy into particle energy is directly proportional to the light transit time L_o/c. Total EM energy is normalized by $E_o = 10^3$ m.

(A color version of this figure is available in the online journal.)

Our underlying astrophysical picture is that some central engine activity lasting tens of seconds launches an intense EM pulse of length $\sim 10^{12}$ cm and energy $\sim 10^{51}$ ergs, loaded with low-density e^+e^- plasma so that $\Omega_e/\omega_{pe} \gg 1$. This intense EM pulse initially propagates through a collapsar envelope as a non-relativistic MHD pulse, since the ambient density is high and the formal Alfven speed $v_A = B/(4\pi\rho_p)^{1/2} \ll c$ (ρ_p = ambient gas mass density, in this section we write out c explicitly). But the pulse eventually reaches a point where the ambient density is so low that $v_A \geqslant c$, and the MHD pulse "breaks out" into a kinetic EM expansion similar to the scenario studied by Liang & Nishimura (2004). This PF "breakout" triggers the CPFA and rapid conversion of EM energy into particle energy. We have performed PIC simulations of relativistic strongly magnetized magnetosonic pulses propagating down steep density gradients. The preliminary results seem to support the above "breakout" picture. We emphasize that in this case the GRB "ejecta" are

just a bundle of EM energy with current-carrying leptons (e^+ or e^-) which act as radiation agents with little inertia.

For long GRBs, it is useful to scale the burst parameters with the following benchmark values (Fishman & Meegan 1995; Preece et al. 2000): total energy $E_{51} = E_{\rm tot}/10^{51}$ erg, burst duration $T_{30} = T/30$ s, prompt-γ emission distance $R_{14} = R/10^{14}$ cm. We approximate the EM pulse as a quasi-spherical shell with thickness $\Delta R = cT = 10^{12}$ cm T_{30} (in this section we write out c explicitly) and solid angle $\Omega_{4\pi} = \Omega/4\pi$. To simplify the model, we assume that the shell is uniform with mean field B and mean lepton ($e^- + e^+$) density n. All physical quantities are measured in the "lab frame", which we assume to be the rest frame of the GRB central engine. In reality, the field, density, and particle momentum profiles are highly structured due to current instabilities (Liang & Nishimura 2004), and the following parameters primarily refer to those leptons with Lorentz factor near $\Gamma \sim$ the peak of the momentum distribution function $\sim \langle\gamma\rangle$ (Figure 2, Liang & Nishimura 2004 showed that $\Gamma \sim$ the group velocity Lorentz factor of EM pulse $= (1 - v_w^2)^{-1/2}$). PIC simulations suggest that at late times, particle energy $E_{\rm particle} \sim 0.6E_{\rm tot}$, EM energy ($= 2E_{\rm B}$) $\sim 0.4E_{\rm tot}$ (Liang et al. 2003). Let $N =$ total number of leptons ($e^+ + e^-$) in the pulse. In cgs units, we have dimensionally

$$N\Gamma mc^2 \sim 6 \times 10^{50}\ E_{51} \tag{11}$$

$$B^2 \Delta R R^2 \Omega \sim 16\pi \times 10^{50}\ E_{51}. \tag{12}$$

Equation (12) gives

$$B \sim 2 \times 10^5\ {\rm G}\left(R_{14}^{-1}\ \Omega_{4\pi}^{-1/2}\ E_{51}^{1/2}\ T_{30}^{-1/2}\right). \tag{13}$$

Next we estimate Γ by invoking Equation (10):

$$\Gamma \sim 1.2 \times 10^5 \left(f^{1/3}\ R_{14}^{1/3}\ \Omega_{4\pi}^{1/6}\ E_{51}^{-1/6}\ T_{30}^{1/6}\ \alpha_{.1}^{-4/3}\right), \tag{14}$$

where we have scaled sinα with 0.1: $\alpha_{.1} = \sin\alpha/0.1$. Hence $\varepsilon \sim 1/\Gamma \ll \sin\alpha$ and our assumption of ignoring ε in Equation (6) is justified. Using this in Equation (11), we find

$$N \sim 6 \times 10^{51} \left(f^{-1/3}\ R_{14}^{-1/3}\ \Omega_{4\pi}^{-1/6}\ E_{51}^{7/6}\ T_{30}^{1/6}\ \alpha_{.1}^{4/3}\right). \tag{15}$$

Combining Equations (8), (13), and (14), we obtain the value of the spectral break energy, taken as the critical frequency corresponding to peak Lorentz factor Γ (Figure 2):

$$E_{pk} = h\omega_{cr}/2\pi \sim 490\ {\rm keV} \times \left(f^{2/3}\ R_{14}^{-1/3}\ \Omega_{4\pi}^{-1/6}\ E_{51}^{1/6}\ T_{30}^{-1/6}\ \alpha_{.1}^{-2/3}\right). \tag{16}$$

Interestingly, this value, which is derived from first principles using the CPFA model, lies in the range of typical spectral break energies of long GRBs in the host-Galaxy frame: $E_{pk} \sim 250$ keV $(1+z) \sim 500$ keV for $z \sim 1$ (Preece et al. 2000). Equation (16) depends only weakly on R, E, T, and Ω. For example, if the jet opening angle $\sim$ few degrees, $\Omega \sim 10^{-2}$, E_{pk} can increase by a factor of 3. If $R \sim 10^{15}$ cm, E_{pk} is reduced by a factor of 2. Since f and α can vary by a factor of $\sim$10, E_{pk} can vary by a factor of $\sim$5. All of these variations are consistent with the observed spread of E_{pk} (Preece et al. 2000). It would be interesting to explore the implication of Equation (16) for the Amati–Ghirlanda-type relations (Amati et al. 2002; Ghirlanda et al. 2004) by studying the dependence of T, α, f etc. on the total energy E. We emphasize that conventional synchrotron models of GRBs do not predict values of E_{pk} from first principles since the acceleration mechanism is not specified.

From Equation (15), we obtain the mean lepton density

$$n = N/(\Omega \Delta R R^2) \sim 5 \times 10^{10} \times \left(f^{-1/3}\ R_{14}^{-7/3}\ \Omega_{4\pi}^{-1/6}\ E_{51}^{7/6}\ T_{30}^{-7/6}\ \alpha_{.1}^{4/3}\right) \tag{17}$$

and the magnetization

$$\Omega_e/\omega_{pe} \sim 250\left(f^{1/6}\ R_{14}^{1/6}\ \Omega_{4\pi}^{-5/12}\ E_{51}^{-1/12}\ T_{30}^{1/12}\ \alpha_{.1}^{-2/3}\right) \gg 1, \tag{18}$$

which justifies our EM-domination assumption. At this density the pairs are completely collisionless (Coulomb mean free path $> 10^{20}$ cm). We note that the local acceleration time of an individual lepton, using the above values of B, Γ and sinα, is very short: $t_{\rm acc} = t_{\rm rad} \sim 10^{-2}$ s, which means that the leptons quickly achieve their asymptotic Lorentz factor Γ after PF breakout. However, the cooling/dissipation time of the overall EM pulse is determined by the time to convert the global EM energy into lepton energy, which is proportional to the light transit time across the shell thickness $\Delta R/c$ (Figure 7). Moreover, radiation emitted by the front and back of the plasma pulse also arrives at the detector with a time delay of $\Delta R/c$. These two effects combine to make the GRB duration measured by the detector $\sim \Delta R/c = 30$ s (Figure 7), irrespective of the short acceleration time of individual leptons. We note that 10^{12} cm corresponds to $\sim 10^{14}$ gyroradii, and the acceleration length of $\sim 3 \times 10^8$ cm still equals 10^{10} gyroradii. Both scales are much larger than the largest PIC simulations we have performed ($\sim 10^7$ gyroradii). However, we emphasize that the only physics invoked to derive the acceleration and radiation cooling rates are all scale invariant. Figure 7 also demonstrates the scalability of the overall energy conversion rate. Hence we are reasonably confident that our kinetic results can be applied to macroscopic astrophysical systems.

However, one puzzle remains: why and how does the EM pulse decide to dissipate at $R \sim 10^{14}$ cm from the central engine, two orders of magnitude larger than the EM pulse width and six orders of magnitude larger than the lepton acceleration length?We speculate that it may be the GRB environment, which determines this dissipation distance. Here we venture a speculative but plausible scenario that gives rise to such a far away dissipation site from the central engine. In reality, the PF "breakout" takes place not at a sharp star-vacuum boundary but in an external density gradient whose scale height is much larger than the pulse width or acceleration length. Hence we speculate that Equations (9) and (10) are valid only when the ambient ion mass density drops below the internal pair mass density. Otherwise the EM expansion and particle acceleration would be strongly inhibited by the ambient ion inertia. In the collapsar model, the GRB progenitor is likely surrounded by a Wolf–Rayet wind whose mass density $\sim {\rm A}.5 \times 10^{11}$ r^{-2} g cm^{-1} (Chevalier & Li 2000), where the parameter A depends on the mass-loss rate. Hence the PF "breakout" distance, using the pair density of Equation (17), becomes $r_{\rm breakout} \sim {\rm A}^{1/2} 10^{14}$ cm. In other words, the PF breakout and lepton acceleration are inhibited by ion inertia of the progenitor wind, until the PF reaches an ambient ion mass density of $\leqslant 5 \times 10^{-17}$ g.cm^{-3}, which only occurs at a distance $\geqslant {\rm A}^{1/2} 10^{14}$ cm. Figure 8 illustrates the relevant scales discussed in this scenario.

8. DISCUSSIONS AND SUMMARY

We have shown in this paper that when electrons/pairs are accelerated by a comoving Poynting flux with $\Omega_{\rm e}/\omega_{pe} > 1$, the

Q6

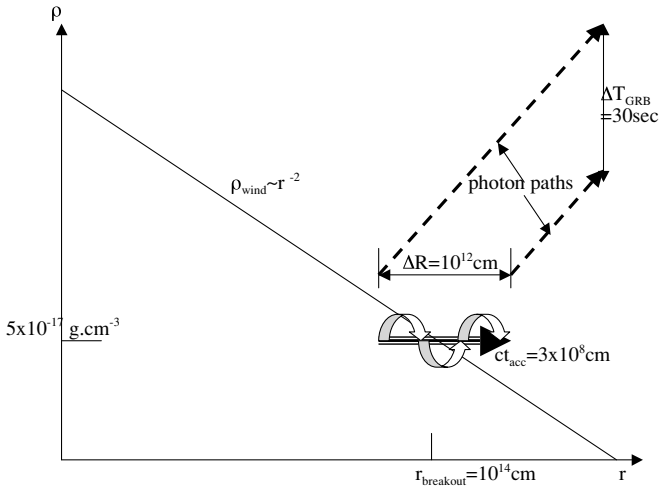

Figure 8. Schematic diagram illustrating the different physical scales in the "breakout" of a PF from a Wolf–Rayet wind model for long GRBs. The wavy arrow denotes the (lab-frame) PF pulse width ($\Delta R = 10^{12}$ cm) along the observer line of sight. The PF breakout distance ($\sim 10^{14}$ cm) is determined by the radius at which the ambient wind mass density drops below the PF internal pair mass density ($\sim 5 \times 10^{-17}$ g cm^{-3}). Despite the short acceleration length ($\sim 3 \times 10^8$ cm) of individual leptons as the pulse emerges, the detector-measured GRB duration at infinity is determined by the overall transit time $\sim \Delta R/c = 30$ s of the pulse passing through $r_{\rm breakout}$ and the light paths between the front and back of the PF pulse (upper-right spacetime diagram).

intrinsic radiation power and critical frequency can be estimated analytically, and the values measured in the laboratory frame are much below those expected from synchrotron in a static field. This is because the EM field is almost comoving with the high-energy particles and the particle paths are quasi-rectilinear. We apply our formulas to a simple PF "breakout" model of classical long GRBs, and find that the predicted spectral break energy agrees with the range of observed E_{pk} values.

Besides the CPFA mechanism, there are many other Poynting flux scenarios that can lead to nonthermal particle acceleration. For example, electron acceleration by longitudinal wake fields generated by PF in an underdense plasma (similar to laser accelerators in the laboratory, Tajima & Dawson 1979) may occur in special astrophysical situations. We have also not considered Poynting flux dominated by Alfven and whistler waves. In general, waves of all types can transfer energy to electrons via resonant scatterings (Boyd & Sanderson 1969). But resonant interactions tend to only act on a small fraction of the electrons at any time, whereas the ponderomotive force of CPFA accelerate the bulk of the plasma in a sustained manner, and transfer most of the EM energy to particles. PF acceleration of e–ion plasmas is more complex than e^+e^- plasmas due to charge separation (Nishimura et al. 2003). Their radiation output will be studied in a separate paper.

This work was partially supported by NSF AST0406882 and NASA NNG06GH06G.

REFERENCES

Abdo, A. A., et al. 2009, Science, 323, 1688
Amati, L., et al. 2002, A&A, 390, 81
Birdsall, C. K., & Langdon, A. B. 1991, Plasma Physics via Computer Simulation (Bristol: Institute of Physics Publishing)
Boyd, T., & Sanderson, J. 1969, Plasma Dynamics (New York: Barnes & Noble)
Chevalier, R. A., & Li, Z. Y. 2000, ApJ, 536, 195
Dermer, C., & Boettcher, M. 2002, ApJ, 564, 86
Dermer, C., & Chang, J. 1999, ApJ, 512, 699
Dermer, C., et al. 2000, ApJ, 537, 255, 785
Dermer, C., et al. 2003, Nature, 424, 749
Fenimore, E., et al. 2002, in AIP Conf. Proc. 662, ed. G. Ricker & Vanderspek (New York: AIP)
Fishman, G., & Meegan, C. A. 1995, ARA&A, 33, 415
Epstein, R., & Petrosian, V. 1973, ApJ, 183, 611
Gallant, Y., et al. 1992, ApJ, 391, 73
Ghirlanda, et al. 2004a, ApJ, 613, L13
Ghirlanda, et al. 2004b, ApJ, 616, 331
Hartemann, F. V., & Kerman, A. K. 1996, Phys. Rev. Lett., 76, 624
Hededal, C. 2005, PhD thesis, Nordita, Copenhagen
Hoshino, M., et al. 1992, ApJ, 390, 454
Koide, S., et al. 2004, ApJ, 606, 395
Kruer, W., & Estabrook, K. 1985, Phys. Fluids, 28, 430
Kruer, W. L., Valeo, E. J., & Estabrook, K. G. 1975, Phys. Rev. Lett., 35, 1076
Landau, L., & Lifshitz, E. M. 1980, Classical Theory of Fields (London: Pergamon)
Langdon, A. B. 1992, Comput. Phys. Commun., 70, 447
Langdon, B., & Lasinski, B. 1976, Methods. in Computational Physics 16, ed. J. Killeen et al. (New York: Academic), 327
Levinson, A., & Van Putten, M. H. P. M. 1997, ApJ, 488, 69
Liang, E. 2005, Ap&SS, 298, 211
Liang, E., et al. 2003, Phys. Rev. Lett., 90, 085001
Liang, E., & Nishimura, K. 2004, Phys. Rev. Lett., 92, 175005
Liang, E. 2005, in Chiba Japan Conf. Proc., www.astro.phys.s.chiba-u.ac.jp/ca2005/
Liang, E., & Noguchi, K. 2005, RevMexAA, 23, 43
Liang, E., & Noguchi, K. 2006, Il Nuovo Cimento B, 121, 1105
Lloyd, N., & Petrosian, V. 2000, ApJ, 543, 722
Lyubarsky, Y. 2005, in Chiba Japan Conf. Proc., www.astro.phys.s.chiba-u.ac.jp/ca2005/
Lyutikov, M., & Blackman, E. G. 2002, MNRAS, 321, 177
Lyutikov, M., & Blandford, R. 2003, in Proc.1st N. Bohr Summer Inst., ed. R. Ouyed et al., arXiv:astroph/020671
Meszaros, P. 2002, ARA&A, 40, 137
Medvedev, M. 2000, ApJ, 540, 704
Medvedev, M., et al. 2005, ApJ, 562, L75
Nishikawa, K., et al. 2003, ApJ, 595, 555
Nishimura, K., & Liang, E. 2004, Phys. Plasmas, 11, 4753
Nishimura, K., Liang, E., & Gary, S. P. 2003, Phys. Plasmas, 10, 4559
Noguchi, K., et al. 2005, Il Nuovo Cimento, C 28, 381
Piran, T. 2000, Phys. Rep., 333, 529
Preece, R. D., et al. 2000, ApJS, 126, 19
Rybicki, G., & Lightman, A. P. 1979, Radiative Processes in Astrophysics (New York: Wiley)
Silva, L. O., et al. 2003, ApJ, 596, L121
Skjaeraasen, O., et al. 2005, ApJ, 634, 542
Smolsky, M. V., & Usov, V. V. 2000, ApJ, 531, 764
Spitkovsky, A. 2008, ApJ, 682, L5
Tajima, T., & Dawson, J. 1979, Phys. Rev. Lett., 43, 267
Van Putten, M. H. P. M., & Levinson, A. 2003, ApJ, 584, 937
Wilks, S. C., et al. 1992, Phys. Rev. Lett., 69, 1383
Weibel, E. S. 1958, J. Electron. Control, 5, 435
Zhang, B. 2009, ApJ, submitted, preprint